Parking spheres stochastically to model realistic granular packings

Jing Yang,[1] Yuwen Sun,[1] Yang Yang,[1] Yujie Wang,[2,3,4] Bingwen Hu,[1] and Chengjie Xia[1,*]

[1]*Shanghai Key Laboratory of Magnetic Resonance, School of Physics and Electronic Science, East China Normal University, Shanghai 200241, China*

[2]*School of Physics and Astronomy, Shanghai Jiao Tong University, Shanghai 200240, China*

[3]*School of Physics, Chengdu University of Technology, Chengdu 610059, China*

[4]*State Key Laboratory of Geohazard Prevention and Geoenvironment Protection, Chengdu University of Technology, Chengdu 610059, China*

(Received 21 September 2024; accepted 21 January 2025; published 10 February 2025)

The packing geometry of granular solids and other amorphous materials is important to understand their macroscopic behaviors. However, their particle-scale assembly mechanism and the underlying statistical mechanical laws remain unclear. In this work, we develop a model to generate the local packing structures of granular spheres by parking them sequentially and stochastically, and connect the fluctuating structures to the thermodynamic equations of state. The influences of entropy, friction, and mechanical action on local configurations are decomposed with the aid of an effective interparticle interaction, a parking sequence of neighboring particles, and an external potential. Quasiuniversal laws of granular sphere packings observed in previous experiments are replicated by our model and their empirical dependences on particle friction and packing protocol are rationalized. This model provides a general statistical mechanical approach to understanding the nonequilibrium assembly mechanism of amorphous particle packing systems.

DOI: 10.1103/PhysRevE.111.025406

I. INTRODUCTION

Understanding the random assembly mechanism of disordered systems such as metallic glasses, granular materials, and biological tissues is crucial for controlling and utilizing their macroscopic properties [1]. Due to the strongly nonequilibrium nature of these amorphous systems, predicting their packing structures with statistical mechanics is extremely challenging [2–4]. An alternative approach, dating back to the 1960s, attempts to explain the structural characteristics of disordered configurations through simple stochastic geometric models [5]. However, the packing configurations predicted by many such approaches are dissimilar to realistic ones due to their overly simplified assumptions [6,7], and their connections with statistical mechanics are ambiguous. Among these models, a relatively effective "granocentric" model for jammed spherical particles is capable of elucidating packing structural fluctuations, but cannot reproduce actual packing configurations [8]. By connecting Voronoi cell geometry and Edwards' volume ensemble theory [9], Makse and co-workers have established a solvable framework for the equations of state (EOS) of granular particles, but the microscopic packing configurations are coarse-grained [10]. Despite a number of previous attempts [11–13], a theoretical approach for particle packing systems that can predict both local structures and macroscopic EOS is lacking, and consequently, the fundamental statistical mechanics underlying the stochastic process of building an amorphous structure remains unclear.

In this article, we upgrade the original parking model, which builds a packing configuration through stochastic sequential adding of particles around a central particle [14], and use it to study granular sphere packings as a model amorphous solid. In this improved model, we introduce an effective temperature to tune the packing structural fluctuations, and develop a phenomenological strategy to account for the influences of particles' frictional contacts. Using this model, we successfully reproduce ensembles of local packing structures that conform to some newfound experimental rules of granular sphere packings, including a set of roughly protocol-independent and friction-independent EOS of (rescaled) structural variables, as well as a nonmonotonic evolution of contact fabric anisotropy of packings under shear [15,16]. By revealing the statistical mechanical nature of the stochastic geometric approach, our model rationalizes these universal micromechanical phenomena of granular materials, and could aid in establishing a general structural and mechanical understanding of amorphous solids [4,17].

II. MODEL

We begin by providing an overview of the configuration-generating procedure in our model before presenting its specific components and determining model parameters with experimental results. As shown in Fig. 1, in the first step, random gap distances ε between the central sphere and its N candidate neighbors are created according to an effective interparticle potential, and listed as $\{\boldsymbol{\varepsilon}\} = \{\varepsilon_1, \varepsilon_2, \ldots, \varepsilon_N\}$. Secondly, we decide whether this sequence is accepted to generate a configuration based on a criterion mapped phenomenologically onto the friction-related mechanical stability of a granular packing. Thirdly, the candidate neighbors with ε_i are parked sequentially around the central sphere at stochastic

*Contact author: cjxia@phy.ecnu.edu.cn

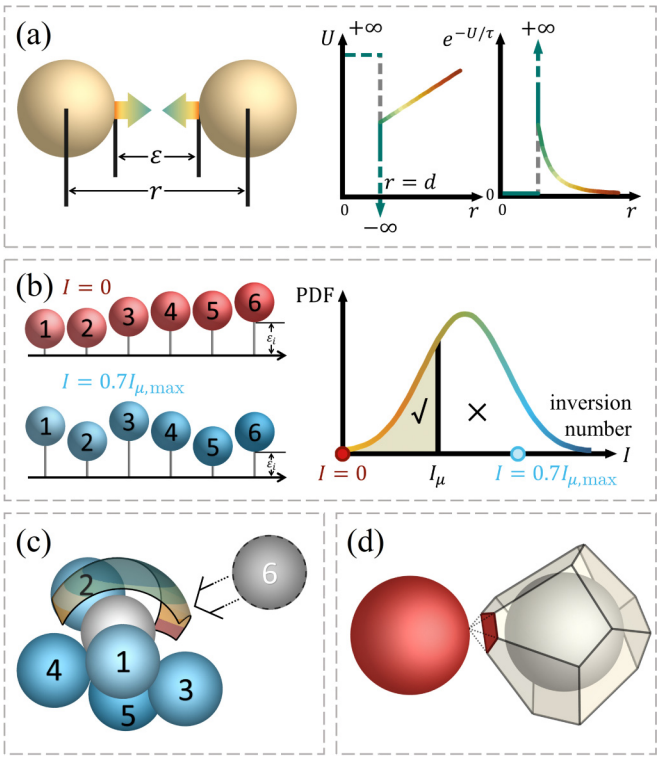

FIG. 1. Schematics for configuration-generating steps: (a) generate random gap distances according to the Boltzmann weight of a potential, (b) select sequences with a threshold of their inversion number, (c) park neighbors around the central sphere sequentially and stochastically, and (d) add outer-shell neighbors to complete the Voronoi cell.

angular positions, weighted by the Boltzmann distribution of the effective potential. Lastly, we continue to park several outer-shell neighbors until the Voronoi cell volume of the central sphere no longer changes. A pseudocode for generating the configurations can be found in Appendix A.

A. Effective interparticle potential

The first key component of our model is an effective potential of mean force between neighboring particles in a dense packing of hard spheres, representing the effect of surrounding particles on two near neighbors that pushes them together under confining pressure [18]. For noncontact neighbors, we denote the effective attraction between two spheres as $U_n(r)$, where $r = \varepsilon + d$ is the distance between sphere centers (i.e., the radial position), ε is the surface gap distance, and d is the sphere diameter. We assume the simplest linear attractive potential $U_n(r) = F_0 r + U_0$, and we have validated that the following results are weakly dependent on the functional form of $U_n(r)$. For contact neighbors, we use Baxter's potential for sticky spheres to model their interaction, which is an infinitely deep potential well with zero width at $r = d$ [19]. This potential leads to a finite number of contacts required in a jammed packing. Together with the hard-sphere repulsion, the total potential is

$$U(r)/\tau = \lim_{d'\to d} \begin{cases} +\infty, & r < d \\ \ln\left[\tau\left(1-\frac{d'}{d}\right)\right], & d \leqslant r < d' \\ U_n(r)/\tau, & r \geqslant d', \end{cases} \tag{1}$$

and the corresponding Boltzmann factor is

$$e^{-U(r)/\tau} = \frac{d}{\tau}\delta(r-d) + e^{-U_n(r)/\tau}\mathrm{H}(r-d), \tag{2}$$

where δ is the Dirac delta function and H is the Heaviside step function. The Boltzmann constant is set to 1. τ acts as an effective temperature [20], adjusting the relative depth of the potential well between contact and noncontact neighbors in our model. The position for adding a candidate neighbor is decided stochastically according to the Boltzmann weight of the potential energy of placing it at different positions $\boldsymbol{r}_i$ (with $|\boldsymbol{r}_i| = \varepsilon_i + d$): $p(\boldsymbol{r}_i;\tau) \propto \prod_{m=0}^{i-1} \exp[-U(|\boldsymbol{r}_i - \boldsymbol{r}_m|)/\tau]$, where $\boldsymbol{r}_m$ are the positions of previously added neighbors, and $m = 0$ represents the central one. A candidate neighbor would be rejected in the parking process if $p(\boldsymbol{r}_i) = 0$ for all $\boldsymbol{r}_i$, meaning that there is no available space to accommodate this neighbor with surface gap ε_i.

B. Density of states of surface gap distance

The second important element of the model is a density of states (DOS) of the surface gap distance, which ensures that our model explores the correct configurational space of a granular packing. A natural expectation for our model is that the packing configurations generated with $\tau = +\infty$ are equivalent to the random loose packing (RLP) state, which is characterized by an infinite configurational temperature according to Edwards' volume ensemble theory [9,15]. However, model-generated configurations would have no contacts (i.e., neighbors with $\varepsilon = 0$), which contradicts the RLP if $\{\boldsymbol{\varepsilon}\}$ is generated with $\tau = +\infty$ simply according to Eq. (2). To resolve this discrepancy, we introduce an additional constant probability $P_{c,0}$ for contact neighbors into the model, which represents the DOS of gap distance at $\varepsilon = 0$. For the same reason, we introduce $g_n(\varepsilon)$ as the gap distance DOS for noncontact neighbors, which is essentially the probability distribution function (PDF) of ε at RLP, to generate a nonflat PDF of ε that aligns with experiment results [21,22].

Combining this DOS and the Boltzmann factor, we obtain the probability density of finding a noncontact neighbor at radial position r:

$$p_n(r)dr = \Xi^{-1}\int_r^{r+dr} g_n(x-d)e^{-U_n(x)/\tau}x^2dx. \tag{3}$$

The total probability of finding a noncontact neighbor is $P_n = Q_n/\Xi$, where $Q_n(\tau) = \int_d^{R_s} g_n(x-d)e^{-U_n(x)/\tau}x^2dx$ and R_s is the outside radius of the shell. The probability of finding a contact neighbor is $P_c + P_{c,0}$ with

$$P_c = \Xi^{-1}\int_d^{R_s} \frac{d}{\tau}\delta(r-d)r^2dr = \frac{d^3}{\tau\Xi} \tag{4}$$

contributed by the Baxter's potential. The normalization factor $\Xi(\tau) = (Q_n + d^3\tau^{-1})/(1-P_{c,0})$ keeps $P_n + P_c + P_{c,0} = 1$. Gap distances in $\{\boldsymbol{\varepsilon}\}$ are generated randomly according to

the contact probability (i.e., $P_{c,0} + P_c$ for $\varepsilon = 0$) and the PDF of nonzero ε [i.e., Eq. (3)].

In this work, we assume a power-law DOS of ε: $g_n(\varepsilon) = G\varepsilon^{-\alpha}$ for $\varepsilon > 0$ and $g_n(0) = 1$, which is inspired by the power-law gap distance distributions of jammed hard spheres and granular disks [23–26]. The proportional factor G can be arbitrary because scaling $G \to kG$, $\tau \to \tau/k$, and $U_n \to U_n/k$ would not change the ratio between d/τ and $g_n e^{-U(r)/\tau}$ and thus keep all following results unchanged [see Eq. (2)]. Therefore, G essentially sets the unit of the effective temperature and potential. We set $G = 2.63 \times 10^{-3}$, which provides a very simple numerical relationship between τ and compactivity χ, i.e., the effective temperature in Edwards' volume ensemble theory for granular packings (see below).

C. Mapping between parking sequences and particle friction

The final component of our model is the acceptance criterion for gap distance sequences, which allows this geometric model to capture some mechanical properties of realistic granular materials. A gap distance sequence $\{\boldsymbol{\varepsilon}\}$ is quantified by its inversion number I, which is the number of pairs in reverse order (i.e., $\varepsilon_i > \varepsilon_j$ for $i < j$), and it is accepted for generating configurations only if $I \leqslant I_\mu$. The threshold I_μ is mapped phenomenologically onto the friction coefficient of granular particles for the following reasons. First, in realistic granular packings, looser configurations with larger average gap distance are more likely to be mechanically stable for more frictional particles. Analogously, model-generated configurations with a larger I_μ tend to have larger average gap distances, because neighbors with large ε are parked earlier in a sequence with larger I. Second, a granular packing can remain stable if the friction coefficient were increased, and the reverse is not true. Correspondingly, configurations generated with a smaller I_μ are naturally a subset of those generated with a larger I_μ owing to the threshold definition. Therefore, we can map a granular sphere packing onto a configuration generation process with I_μ in between the two limits: $I_\mu = 0$ for a frictionless system, corresponding to sequential parking of neighbors with increasing ε_i, and $I_\mu = I_{\mu,\max}$ for the most frictional system modeled with neighbor parking with completely random sequences. $I_{\mu,\max} = N(N-1)/2$ is the maximum possible inversion number.

D. Determination of model parameters

All model parameters are determined by comparing the $Z \sim \Phi$ EOS of model-generated configurations with the corresponding empirical experimental results. Here, Z represents the average contact number, and Φ denotes the average value of local packing fractions φ, i.e., the ratio between the volume of a sphere and its Voronoi cell volume. First, we set $R_s = 2d$ as approximately the largest centroid-to-centroid distance between a central particle and its Voronoi neighbors in granular sphere packings [21]. Second, we set $\tau = +\infty$ to determine the three parameters N, $P_{c,0}$, and α of the gap distance DOS separately from those of the potential, because the specific form of $U(r)$ is irrelevant in this limit. The packing states generated with $\tau = +\infty$ correspond to the RLP states, which have two empirical bounds for spheres with different friction coefficients [27,28]: for infinitely frictional and cohesionless spheres, the average packing fraction $\Phi_{\mathrm{RLP}} \approx 0.55$ and the average contact number $Z_{\mathrm{RLP}} = 4$, and for frictionless spheres, $\Phi_{\mathrm{RLP}} \approx 0.64$ and $Z_{\mathrm{RLP}} = 6$. [Here, it is presumed that the RLP state for frictionless spheres should be very close to the random close packing (RCP), as the mechanically stable states in the landscape of frictionless hard spheres are dominated by the densest ones [16].] Numerical calculations show that the range of Z_{RLP} majorly depends on N and $P_{c,0}$, while Φ_{RLP} relies primarily on α. Thus, we can tune these parameters basically independently to match Z_{RLP} and Φ_{RLP} calculated with $I_\mu = I_{\mu,\max}$ and 0 to their respective bounding values, and obtain the optimized values: $N = 17$, $P_{c,0} = 0.36$, and $\alpha = 0.61$. The potential parameters F_0 and U_0 are determined at last. We explore the parameter space of F_0 and U_0 and find the optimized pair $F_0 \approx 0.38$ and $U_0 \approx 0.88$ that makes the average packing fraction Φ_{RCP} of RCP states (with $Z_{\mathrm{RCP}} = 6$ by definition) calculated with all different values of I_μ close to the empirical value 0.64.

III. RESULTS

A. Packing structural characterizations

We vary τ and I_μ to model different packing states of granular spheres with different friction coefficients, and generate 2×10^4 configurations for each parameter pair. To verify that the model-generated structures are quantitatively close to those of realistic granular spheres, we calculate the following two distributions to characterize the relative positions of neighboring particles of each central sphere, and their evolutions with Φ and I_μ. The first is an angular correlation function, which is the PDF $f(\theta)$ of the angle θ between the connections of the centroid of the central sphere and the centroids of a pair of Voronoi neighbors [Figs. 2(a) and 2(c)]. The second one is the PDF of a shape index of the Delaunay tetrahedra, defined as $\epsilon = \varepsilon_{\max}/d - 1$, where $\varepsilon_{\max}$ is the length of the longest edge of a Delaunay tetrahedron [Figs. 2(b) and 2(d)]. It can be noticed that all these characterizations of multiparticle structural correlations align with previous results on granular sphere packings [29,30], and jammed frictionless hard spheres as well [31]. For model-generated configurations at the same Φ (I_μ), the local structures become slightly less ordered as I_μ (Φ) decreases, reflected in the decreasing probability of finding local structures close to a regular triangle or a regular tetrahedron. Obviously, achieving a lower Φ at a fixed I_μ requires a higher effective temperature, and equivalently, it needs a higher τ to introduce sufficient randomness, ensuring that Φ remains unchanged in ensembles with smaller I_μ. The evolution trends of local structural ordering with varying packing fraction and friction coefficients are consistent with previous results [29,30,32,33].

B. $Z \sim \Phi$ equation of states

In this section, we focus on the relationship between average contact number Z and packing fraction Φ, and provide some understandings on this central EOS of granular materials with our model. As shown in Fig. 3(a), the $Z \sim \Phi$ EOS of model-generated configurations are very similar to the experimental results [see Fig. 4 of Ref. [15]]. Notably, Φ_{RCP}

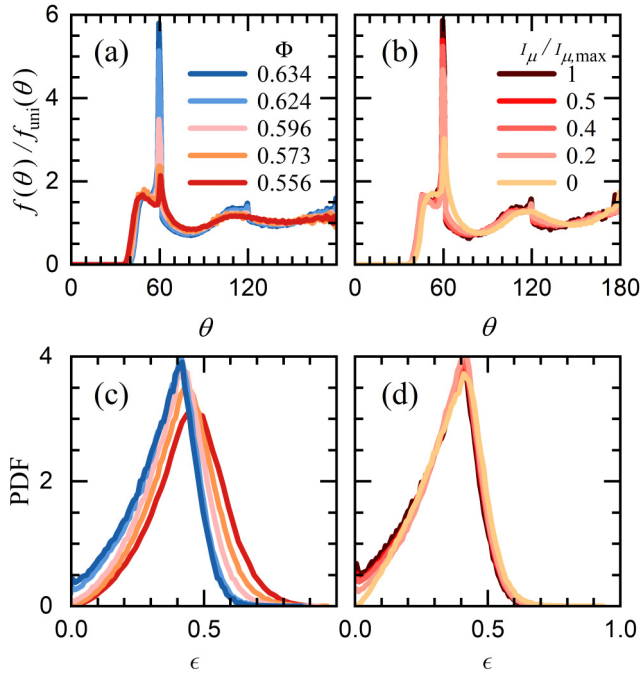

FIG. 2. (a),(b) The angular correlation functions of Voronoi cell neighbors, normalized by the uniform angular distribution $f_{\rm uni}(\theta) = \sin\theta/2$. (c),(d) PDFs of the Delaunay cell shape index ϵ. Curves in (a) and (c) correspond to configurations generated with $I_\mu = I_{\mu,\max}$, modeling spheres with a very large friction coefficient, and different average packing fractions Φ obtained with varying effective temperatures τ. In (b) and (d), each curve corresponds to an ensemble of configurations obtained with a different I_μ, and approximately the same $\Phi \approx 0.637$ by adjusting τ separately.

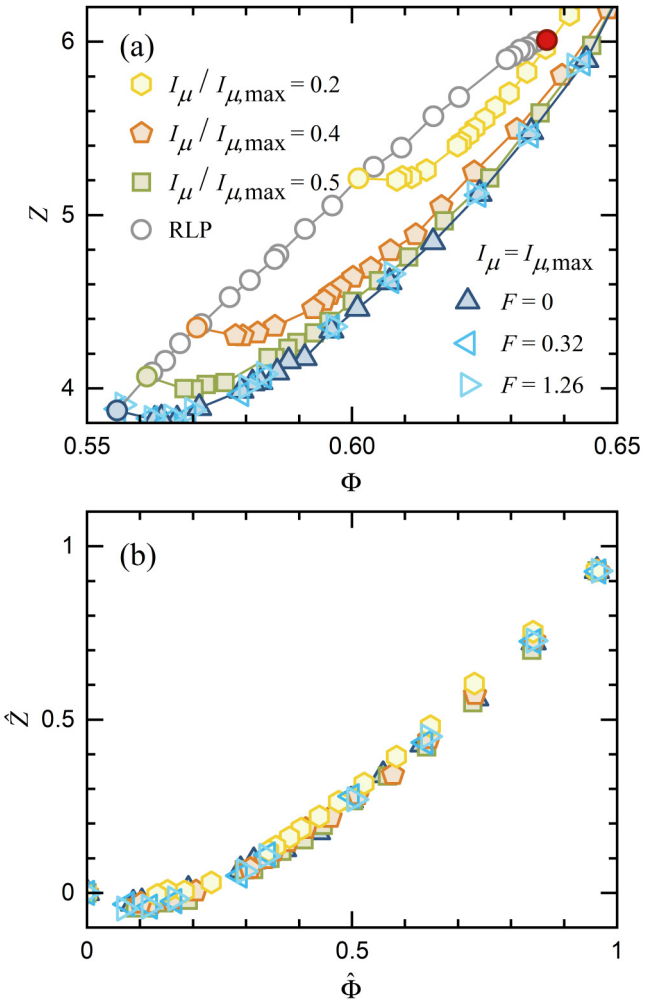

FIG. 3. (a) Relationships between Z and Φ. The RLP data are generated with $\tau = +\infty$ and different I_μ, and are bounded by ($\Phi_{\rm RLP} \approx 0.55$, $Z_{\rm RLP} \approx 4$) and ($\Phi_{\rm RCP} \approx 0.64$, $Z_{\rm RCP} \approx 6$) marked by the blue and red circles. The data points from left to right on each curve for a fixed value of I_μ correspond to $\tau = +\infty$, followed in turn by four evenly spaced temperatures between 0.979 to 0.474, and 13 evenly spaced temperatures between 0.458 to 0.284. Solid symbols represent isotropic configurations with external force $F = 0$, and hollow triangles denote anisotropic configurations with $F = 0.32$ and 1.26. (b) The data points in (a) rescaled by their values at $\tau = \tau^* = 0.295$ (whose packing states are close to RCP) and $\tau = +\infty$ (i.e., RLP).

of particles obtained with different I_μ lie in a small range of $(0.637, 0.646)$ instead of at a single point, indicating a subtle role of the friction of granular materials in selecting packing states, although the frictional forces could be weak in dense packings [34]. Slightly different $\Phi_{\rm RCP}$ in this range have also been observed in several previous studies [35–37]. Furthermore, the broader range of Φ obtained with a larger threshold I_μ is clearly due to more configurations being accepted, highlighting the role of friction in selecting packing states in the configurational space [10,15,16,38]. The trends of Z and Φ as functions of varying I_μ can be found in Appendix B.

Interestingly, we observe a mild decrease in the average contact number during the initial densification above RLP regardless of I_μ [Fig. 3(a)]. This phenomenon has also been observed in a previous experiment on granular spheres with different friction coefficients [15], as well as in a numerical study of jammed packings of frictionless spheres [31]. To understand this phenomenon, we further calculate the average number N_c of neighbors that are very close to the central particles, i.e., those with $\varepsilon \leqslant \varepsilon_t$. Similar to Z, N_c also evolves nonmonotonically with $1/\tau$, when $\varepsilon_t \lesssim 10^{-3}d$ [Fig. 4(a)]. (Note that Φ always increases as τ decreases.) Therefore, this particular behavior involves both contact and noncontact neighbors, suggesting a geometric rather than mechanical origin. We also calculate the average gap distance $\langle\varepsilon\rangle$ for neighbors with $\varepsilon \leqslant \varepsilon_t$, and consistently, we observe the counterintuitive nonmonotonic evolution of $\langle\varepsilon\rangle$ versus $1/\tau$ for $\varepsilon_t \lesssim 10^{-2}d$ [Figs. 4(c)–4(e)].

We propose that the nonmonotonic evolution of Z and the number of very close noncontact neighbors with Φ originates from the different evolving behaviors of radial and angular correlations of neighbors around a central sphere during densification. According to our model, the average radial position of a candidate neighbor is determined by its interaction with the central particle, while its angular position, or equivalently, its average distance from other neighbors of the same central particle, is affected by the multiple interactions between it and other preexisting neighbors. Hence, the average radial position $\langle r_c\rangle$ of the candidate neighbors and

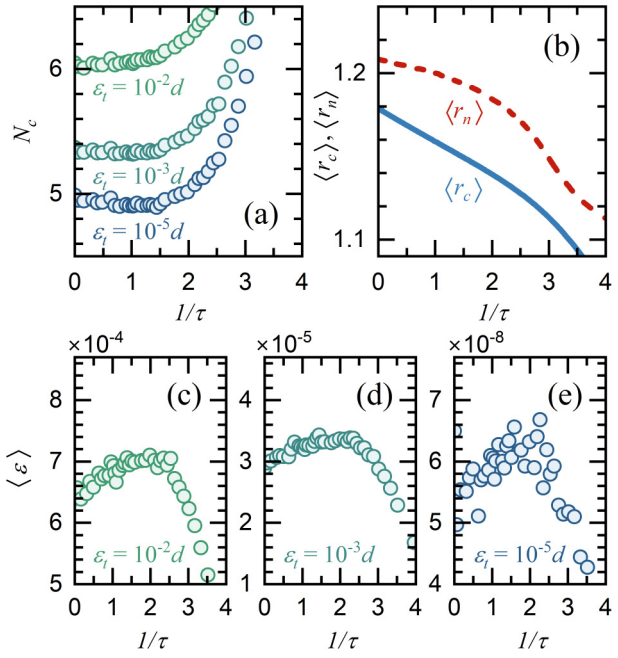

FIG. 4. (a) Average number N_c of close neighbors whose gap distances $\varepsilon \leqslant \varepsilon_t$ as a function of $1/\tau$. Data of three different values of ε_t are shown. (b) Average radial position of the candidate neighbors $\langle r_c\rangle$ (solid line) and average neighbor-neighbor distance $\langle r_n\rangle$ (dashed line) vs $1/\tau$. (c)–(e) Average gap distance of close neighbors as a function of $1/\tau$, with $\varepsilon_t = 10^{-2}d$ (c), $\varepsilon_t = 10^{-3}d$ (d), and $\varepsilon_t = 10^{-5}d$ (e), respectively.

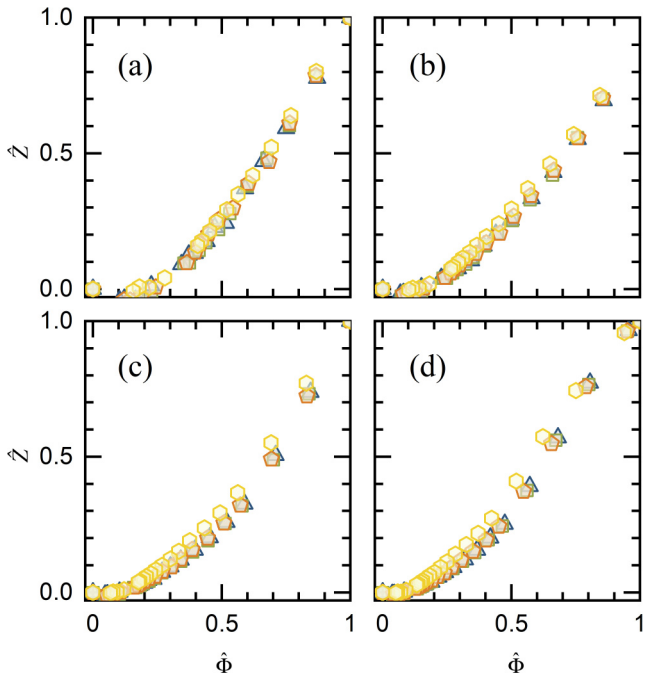

FIG. 5. The $\hat{Z} \sim \hat{\Phi}$ EOS obtained with (a) $\tau^* = 0.316$ (the corresponding average high-Φ bound is about 0.632), (b) $\tau^* = \tau_0 = 0.259$, (c) $\tau^* = 0.189$, and (d) $\tau^* = 0.063$.

the average neighbor-neighbor distance $\langle r_n\rangle$ should exhibit unequal dependence on the effective temperature τ. Specifically, when $1/\tau$ increases slightly from zero, $\langle r_c\rangle$ changes faster than $\langle r_n\rangle$ [Fig. 4(b)]. As a result, the available space for candidate neighbors with $\varepsilon \approx 0$ is reduced upon densification above RLP, and the innermost shell of the neighbors has to expand slightly to accommodate more neighbors and densify the local configuration. At a much lower effective temperature (e.g., $\tau \lesssim 0.5$), the neighbors are already arranged in more angularly ordered configurations, so that the radial correlation is no longer necessary to be sacrificed to accommodate more neighbors. A similar nonaffine local structural deformation of granular sphere packings was studied previously [22]. Note that the model parameters are not intentionally tuned for this particular behavior to emerge, and thus we believe our model captures some crucial structural rearrangement mechanism of jammed spheres.

C. Rescaled $Z \sim \Phi$ relationships

In addition to the packings between RLP and RCP accessible to experiments, our model can probe noncrystalline states with $\Phi > \Phi_{\mathrm{RCP}}$, which are impossible in a global packing, because the sequential parking procedure to generate local configurations lacks the cooperative structural rearrangements required for crystallization [39,40]. These states correspond to deeply quenched glassy states beyond the dynamic glass transition point [17]. Interestingly, our model shows that Φ and Z can be rescaled onto an I_μ-independent master curve across a range of packing states extending continuously beyond RCP. The rescaled variables are $\hat{\Phi} = (\Phi - \Phi_{\mathrm{RLP}})/(\Phi^* - \Phi_{\mathrm{RLP}})$ and $\hat{Z} = (Z - Z_{\mathrm{RLP}})/(Z^* - Z_{\mathrm{RLP}})$, with Φ^*, Z^*, Φ_{RLP}, and Z_{RLP} representing the average packing fraction and contact number at $\tau = \tau^*$ and $\tau = +\infty$, respectively [Fig. 3(b)]. The $\hat{\Phi} \sim \hat{Z}$ EOS of different I_μ can be collapsed onto the same curve with different τ^* regardless of whether the high-Φ bound is lower or higher than RCP, yet the collapsing becomes worse if $\tau^* < \tau_c \approx 0.259$ (Fig. 5). We find that this critical temperature marks a boundary between a pure ensemble of disordered configurations and a mixed ensemble of both disordered and icosahedronlike configurations (see below). The average packing fraction corresponding to τ_c is around 0.663. The physical meaning of τ_c would be clearer by relating it to the Edwards' compactivity in the following.

The PDFs of local packing fractions φ of the central spheres of model-generated configurations are shown in Fig. 6(a), where the data of different average packing fractions Φ corresponding to τ higher and lower than τ_c are displayed. The PDF splits into different peaks for configurations generated with τ smaller than a critical temperature $\tau_c \approx 0.259$, which is basically independent of the inversion number threshold I_μ. A detailed structural examination demonstrates that these separated peaks correspond to intact or partial icosahedral clusters [Figs. 6(b)–6(e)]. Therefore, this critical temperature marks a boundary between a pure ensemble of disordered configurations and a mixed ensemble of both disordered and icosahedronlike configurations. Correspondingly, in the limit of $\tau \to 0$, we notice that the $Z \sim \Phi$ EOS for all different I_μ converge to a common point ($Z_{\mathrm{icosa}} = 12$, $\Phi_{\mathrm{icosa}} \approx 0.755$) on the phase diagram, which corresponds to an intact icosahedral cluster.

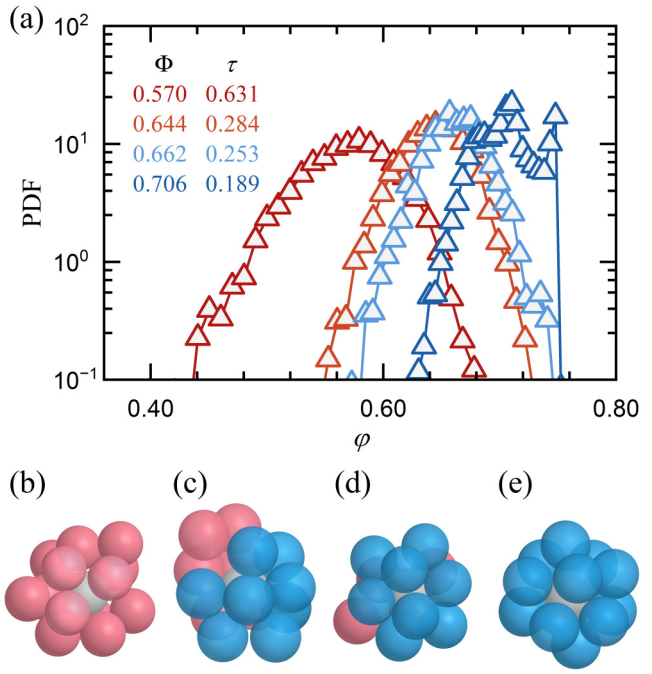

FIG. 6. PDFs of local packing fraction φ of configurations with different average packing fractions and $I_\mu = I_{\mu,\max}$. Different symbols represent configurations with different Φ and τ. (b)–(e) Some typical local packing structures of the central particles, with $\varphi =$ 0.580 (b) and 0.655 (c) belonging to the broad peak of disordered configurations in the PDFs, and $\varphi = 0.687$ (d) and 0.751 (e) belonging to the sharp peaks. Blue spheres indicate part of an icosahedral cluster.

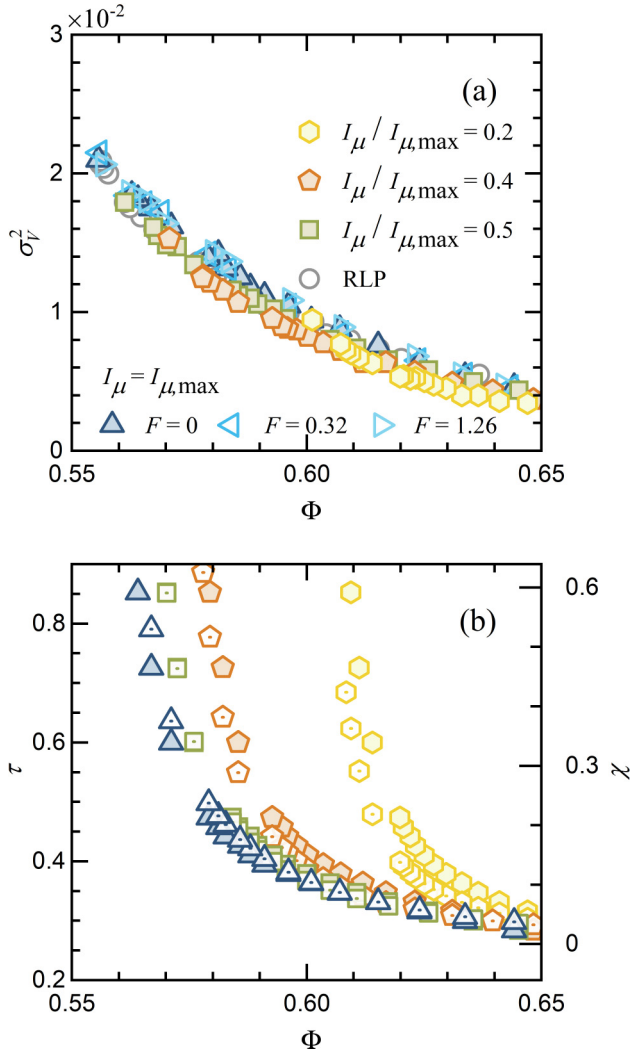

FIG. 7. (a) Variance of Voronoi cell volumes of central spheres vs packing fraction Φ, for different values of I_μ and F. (b) Effective temperature τ in the model (left axis, solid symbols), and the compactivity χ of Edwards' volume ensemble (right axis, symbols with dots at center) as a function of Φ for different values of I_μ.

D. Effective temperatures

To understand the statistical mechanical nature of our model, we connect the effective temperature τ with the Edwards' compactivity χ calculated from the variance of Voronoi cell volumes σ_V^2 according to $\chi^{-1} = V_g \int_{\Phi_{\rm RLP}}^{\Phi} \frac{d\Phi'}{\Phi'^2 \sigma_V^2(\Phi')}$ [41]. V_g is the sphere volume and is set to unity. The model-generated configurations have a roughly I_μ-independent relationship between σ_V^2 and Φ [Fig. 7(a)], which is also consistent with previous experimental results [15,16]. In Fig. 7(b), we plot χ on the right axis together with τ on the left axis as a function of Φ. By tuning the origins of the axes, we can superimpose the curves of $\chi(\Phi)$ roughly onto the corresponding curves of $\tau(\Phi)$ for different I_μ simultaneously. This means a friction-independent linear relationship between the two temperatures: $\chi = \tau - \tau_0$ with $\tau_0 = 0.261$. ($d\chi/d\tau = 1$ because the unit of τ is preset by G.) Note that this relationship fails and χ is ill-defined when $\tau < \tau_0$ due to the mixed disordered-icosahedral phase in this temperature regime. This friction-independent $\chi \sim \tau$ relationship justifies the role of τ as the effective temperature controlling the structural fluctuations. Furthermore, noticeably, the offset τ_0 is basically identical to τ_c obtained above, suggesting that they share the same physical meaning: they are the lowest temperature to generate the ground-state densest disordered sphere packings with zero compactivity, analogous to the glassy close packing state [4,17], and also the critical temperature of a disorder-icosahedral ordering transformation. Interestingly, this low-τ phase exhibits strong structural similarities to the Frank-Kasper phase [42], as it features the structural motif of distorted icosahedral clusters. The local cluster generation process of our model can probe the structural characteristics of this hidden ground amorphous state that is ordinarily hindered by geometric frustration. This is quite similar to the first-order phase transition in trajectory space revealed by a biased simulation [43], as well as the icosahedral ordering transition obtained in curved space, which relieves the frustration [44].

E. Anisotropic structures and their evolution under shear

In the following, we extend the above isotropic model to situations involving a symmetry-breaking mechanical field, e.g., a shear stress. To model the influence of a mechanical action, we add an external energy $U_F = FS\Delta(\varepsilon_i)$ to the total potential of candidate neighbors. $\Delta(\varepsilon_i) = 1$ if $\varepsilon_i = |\boldsymbol{r}_i| - d = 0$ and zero otherwise to model the di-

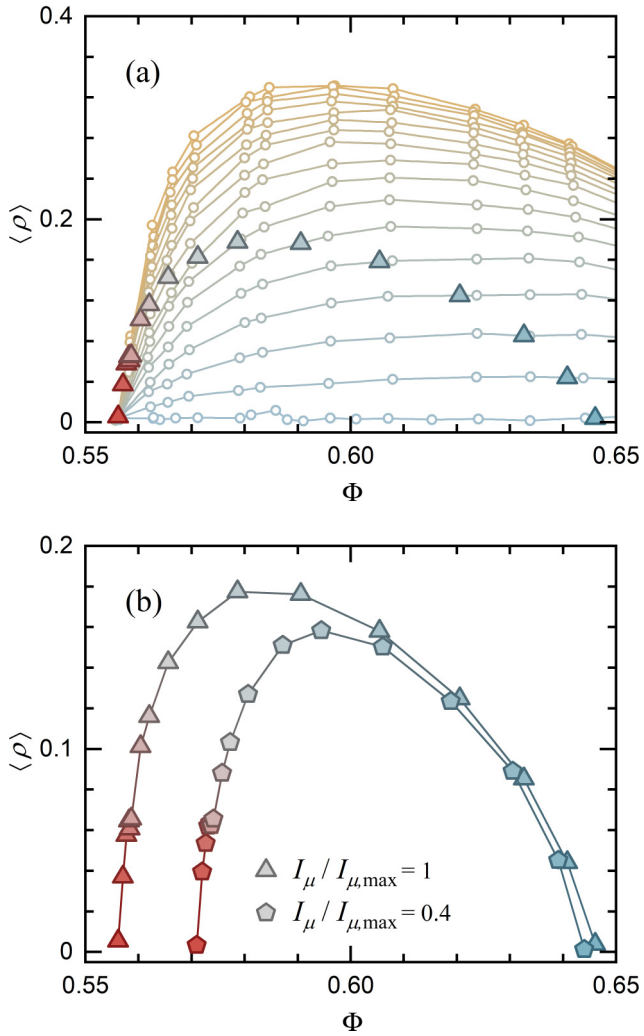

FIG. 8. (a) Average anisotropy index $\langle\rho\rangle$ of the fabric tensor vs packing fraction Φ, calculated by varying the effective temperature τ. Curves from bottom to top correspond to different force strengths F with equal intervals from 0 to 2.5. (b) Evolution of $\langle\rho\rangle$ with Φ for model-generated configurations with $I_\mu = I_{\mu,\max}$ (triangles) and $I_\mu = 0.4I_{\mu,\max}$ (pentagons).

rect mechanical loads on the contacts, which act as the force bearer and indirectly affect the Voronoi cell configurations. This energy couples the strength of the external force F to an order parameter $S = \langle 3\cos^2\theta_i - 1\rangle/2$ of contact orientations with θ_i being the angle between $\boldsymbol{r}_i$ and a fixed major direction of the force. Accordingly, the probability of placing a contact neighbor at $\boldsymbol{r}_i$ becomes $p(\boldsymbol{r}_i) \propto \prod_{m=0}^{i-1} \exp[-U_n(|\boldsymbol{r}_i - \boldsymbol{r}_m|)/\tau]\exp[-U_F(\boldsymbol{r}_i)/\tau]$. Interestingly, as shown in Figs. 3(a) and 7(a), the $Z \sim \Phi$ EOS and the variance of Voronoi cell volume are unaffected by the force field, proving that the correlation between the contact and Voronoi structures of granular spheres is weak [16], and demonstrating the external force's effect in selecting a subset of configurations with anisotropic contact structures. The contact structures are quantified by the fabric tensor $\boldsymbol{A}_f = \langle \boldsymbol{n}_i \otimes \boldsymbol{n}_i\rangle - \boldsymbol{I}/3$ and its anisotropy index ρ as the ratio between the smallest and largest eigenvalues, where $\boldsymbol{n}_i$ is the contact direction (i.e., a unit normal vector on the ith contact point of the central sphere), and $\boldsymbol{I}$ is the unit tensor. As shown in Fig. 8(a), the average anisotropy index $\langle\rho\rangle$ increases with F and evolves nonmonotonically with Φ. This is because the configurations are densely packed at low temperatures, which strongly suppresses anisotropic structures, whereas at high temperatures, entropy dominates over the anisotropic external potential.

We continue to model the dilatancy and heating effect of shearing and study the underlying evolution of local packing structures. To this end, we use an empirical function to fit the relationship between Edwards' compactivity X and shear strain γ obtained in previous experiments [16]:

$$X - X_{\mathrm{RCP}} = \beta'^{-1}(e^{\kappa'\gamma} - 1), \tag{5}$$

where X_{RCP} is the compactivity of the random close packing state as the initial condition of the shear. For the experimental results obtained using two types of spheres with different friction coefficients, we obtain $\kappa' = 10.40$ for the less frictional spheres, and $\kappa' = 9.24$ for the more frictional ones. $\beta' = 38.6$ is also obtained by fitting as a friction-independent constant.

In Refs. [15,16], X is calculated based on the variance of coarse-grained Voronoi cell volumes, that is, the average Voronoi cell volume of a central sphere and its neighbors within a given distance. In the present work, the compactivity χ is calculated from the variance of the volumes of single Voronoi cells, but it is simply proportional to X according to $\chi \approx 0.43X$ [15,45]. Additionally, we assume a proportional relationship between γ and the strength F of the anisotropic potential: $F = E\gamma$. The constant E is set to 3.16 to make the values of the contact fabric anisotropy index calculated with the model close to the experimental results. Together with the relationship $\chi = \tau - \tau_0$ obtained above, we can transform Eq. (5) into:

$$\tau - \tau_{\mathrm{RCP}} = \beta^{-1}(e^{\kappa F} - 1). \tag{6}$$

The parameters rescaled correspondingly are $\beta = \beta'/0.43 = 89.8$, $\kappa = \kappa'/E = 3.29$ for the less frictional system with $I_\mu = 0.4I_{\mu,\max}$, and $\kappa = 2.92$ for the more frictional system with $I_\mu = I_{\mu,\max}$. By interpolating this $\tau \sim F$ relation [Eq. (6)], the $\Phi \sim \tau$ EOS [Fig. 7(b)], and the $\rho \sim F$ relation [Fig. 8(a)], we obtain the evolution of ρ as a function of Φ during a complete shear dilatancy from RCP to RLP [Fig. 8(b)], which is also very similar to previous experimental results [see Fig. 4 of Ref. [16]]. With this model, we can now attribute unambiguously this nonmonotonic evolution of contact fabric anisotropy to the competition between the increasingly strong shear force and the growing randomness due to the rising configurational temperature.

IV. CONCLUSION

In this article, we devise a parking model for a subsystem involving only the first-shell neighbors of a granular packing. The configuration-generating process of the model is analogous to exploring a coarse-grained (free-)energy landscape of hard-sphere glasses or granular sphere packings, with an effective temperature controlling the sampling weights of different microstates. With this model, we separate the effects of configurational temperature, friction, and external force on

granular packing structures, and successfully reproduce and explain some newfound complex and quasiuniversal laws in granular sphere packings. This approach can also be generalized to polydisperse and nonspherical granular materials [46], as well as systems with various intrinsic interactions like soft particles and wet sands [47,48]. Fundamentally, by introducing an effective potential to greatly simplify the many-body correlations in dense particle assemblies, our approach connects the microscopic structures, macroscopic EOS, and generalized statistical mechanics for athermal and glassy systems, and has the potential to be applied to other amorphous solids.

ACKNOWLEDGMENTS

We thank W. Kob for helpful discussions. This work was supported by the National Natural Science Foundation of China (Grants No. 12474193 and No. 12274292).

APPENDIX A: MODEL PSEUDOCODE

The following is a pseudocode of the configuration generation process, where the function INVERSE_NUMBER returns the inversion number of a gap distance sequence.

ALGORITHM 1. Configuration generation process.

Input: effective temperature τ, effective potential $U(r)$, density of state $g_n(\varepsilon)$, inversion number threshold I_μ, sequence length N, sphere diameter d
Output: parked neighbors' coordinates $\{\boldsymbol{r}_m\}$

Create gap distance sequence $\{\boldsymbol{\varepsilon}\}$ using $U(r)/\tau$ and $g_n(\varepsilon)$
repeat
  Randomly arrange $\{\boldsymbol{\varepsilon}\}$
until INVERSE_NUMBER($\{\boldsymbol{\varepsilon}\}$)$\leqslant I_\mu$
$\boldsymbol{r}_m \leftarrow \{\,\}$
for $i = 1, \ldots, N$ //sequential neighbor parking
  Compute Boltzmann weight $p(\boldsymbol{r}_j;\tau)$ for all $\boldsymbol{r}_j$ s. t. $|\boldsymbol{r}_j| = \varepsilon_i + d$
  if $\forall \boldsymbol{r}_j$, $p(\boldsymbol{r}_j;\tau) = 0$ **then**
    continue
  else
    Choose $\boldsymbol{r}_j$ randomly according to $p(\boldsymbol{r}_j;\tau)$
    $\boldsymbol{r}_m \leftarrow \{\boldsymbol{r}_m, \boldsymbol{r}_j\}$
  end if
end for
while $\exists \boldsymbol{r}$, s. t. $|\boldsymbol{r}| = 2d$, $p(\boldsymbol{r};\tau) > 0$ //park outer-shell neighbors
  Create a random gap distance ε and candidate positions $\boldsymbol{r}_j$
  Compute $p(\boldsymbol{r}_j;\tau)$ and randomly choose $\boldsymbol{r}_j$ accordingly
  $\boldsymbol{r}_m \leftarrow \{\boldsymbol{r}_m, \boldsymbol{r}_j\}$
end while

APPENDIX B: Z AND Φ WITH A VARYING I_μ

In Fig. 9, we show the relationships between the average packing fraction Φ, the contact number Z, and I_μ, which should be mapped onto the particle's friction coefficient, for different values of the effective temperature τ. These trends are consistent with previous numerical results regarding the influence of the friction coefficient on granular packing structures [28,49,50].

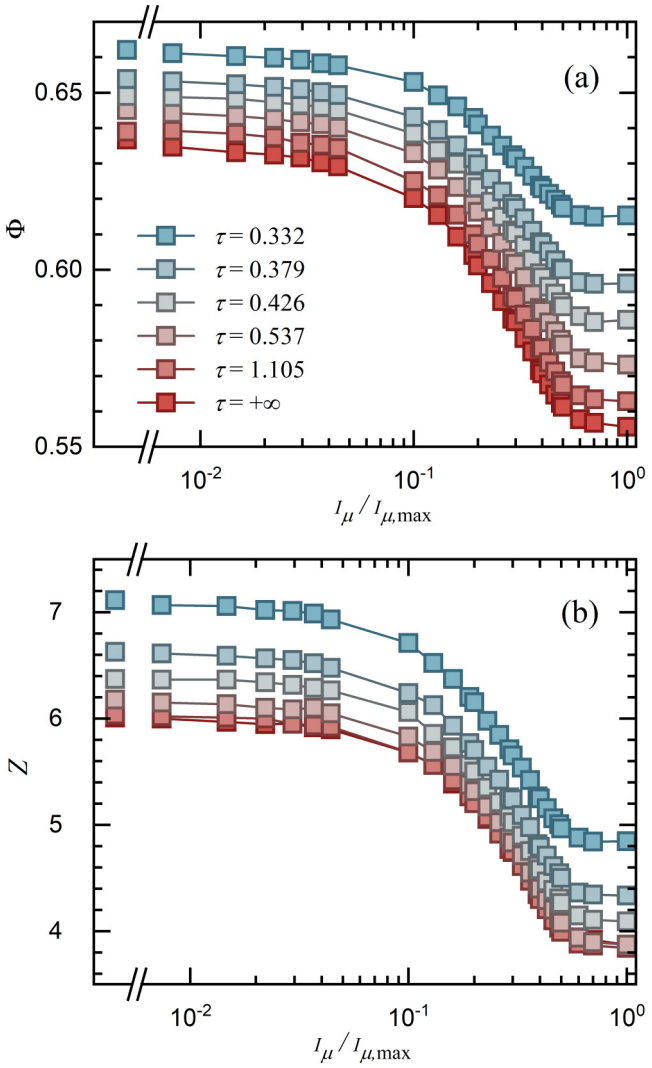

FIG. 9. (a) The average packing fraction Φ and (b) average contact number Z as a function of the inversion number threshold I_μ normalized by $I_{\mu,\max}$. Curves from top to bottom correspond to increasing effective temperatures. The leftmost points on all curves represent the data with $I_\mu = 0$ (i.e., frictionless).

[1] S. Torquato, Perspective: Basic understanding of condensed phases of matter via packing models, J. Chem. Phys. **149**, 020901 (2018).

[2] S. Torquato and F. H. Stillinger, Jammed hard-particle packings: From Kepler to Bernal and beyond, Rev. Mod. Phys. **82**, 2633 (2010).

[3] L. Berthier and G. Biroli, Theoretical perspective on the glass transition and amorphous materials, Rev. Mod. Phys. **83**, 587 (2011).

[4] A. Baule, F. Morone, H. J. Herrmann, and H. A. Makse, Edwards statistical mechanics for jammed granular matter, Rev. Mod. Phys. **90**, 015006 (2018).

[5] J. D. Bernal, A geometrical approach to the structure of liquids, Nature (London) **183**, 141 (1959).

[6] A. Wouterse and A. P. Philipse, Geometrical cluster ensemble analysis of random sphere packings, J. Chem. Phys. **125**, 194709 (2006).

[7] G. Roquier, A century of granular packing models, Powder Technol. **441**, 119761 (2024).

[8] M. Clusel, E. I. Corwin, A. O. N. Siemens, and J. Brujić, A 'granocentric' model for random packing of jammed emulsions, Nature (London) **460**, 611 (2009).

[9] S. F. Edwards and R. B. S. Oakeshott, Theory of powders, Physica A (Amsterdam) **157**, 1080 (1989).

[10] C. Song, P. Wang, and H. A. Makse, A phase diagram for jammed matter, Nature (London) **453**, 629 (2008).

[11] W. M. Visscher and M. Bolsterli, Random packing of equal and unequal spheres in two and three dimensions, Nature (London) **239**, 504 (1972).

[12] C. H. Bennett, Serially deposited amorphous aggregates of hard spheres, J. Appl. Phys. **43**, 2727 (1972).

[13] H. Jacquin, L. Berthier, and F. Zamponi, Microscopic mean-field theory of the jamming transition, Phys. Rev. Lett. **106**, 135702 (2011).

[14] M. L. Mansfield, L. Rakesh, and D. A. Tomalia, The random parking of spheres on spheres, J. Chem. Phys. **105**, 3245 (1996).

[15] Y. Yuan *et al.*, Experimental test of the Edwards volume ensemble for tapped granular packings, Phys. Rev. Lett. **127**, 018002 (2021).

[16] Y. Xing, Y. Yuan, H. Yuan, S. Zhang, Z. Zeng, X. Zheng, C. Xia, and Y. Wang, Origin of the critical state in sheared granular materials, Nat. Phys. **20**, 646 (2024).

[17] G. Parisi and F. Zamponi, Mean-field theory of hard sphere glasses and jamming, Rev. Mod. Phys. **82**, 789 (2010).

[18] J.-P. Hansen and I. R. McDonald, *Theory of Simple Liquids: With Applications to Soft Matter* (Academic, New York, 2013).

[19] R. J. Baxter, Percus-Yevick equation for hard spheres with surface adhesion, J. Chem. Phys. **49**, 2770 (1968).

[20] B. Barboy, On a representation of the equation of state of fluids in terms of the adhesive hard-spheres model, J. Chem. Phys. **61**, 3194 (1974).

[21] K. A. Newhall, I. Jorjadze, E. Vanden-Eijnden, and J. Brujic, A statistical mechanics framework captures the packing of monodisperse particles, Soft Matter **7**, 11518 (2011).

[22] C. Xia *et al.*, Origin of noncubic scaling law in disordered granular packing, Phys. Rev. Lett. **118**, 238002 (2017).

[23] M. Wyart, Marginal stability constrains force and pair distributions at random close packing, Phys. Rev. Lett. **109**, 125502 (2012).

[24] P. Charbonneau, J. Kurchan, G. Parisi, P. Urbani, and F. Zamponi, Fractal free energy landscapes in structural glasses, Nat. Commun. **5**, 3725 (2014).

[25] F. Arceri and E. I. Corwin, Vibrational properties of hard and soft spheres are unified at jamming, Phys. Rev. Lett. **124**, 238002 (2020).

[26] Y. Wang, J. Shang, Y. Jin, and J. Zhang, Experimental observations of marginal criticality in granular materials, Proc. Natl. Acad. Sci. USA **119**, e2204879119 (2022).

[27] G. W. Delaney, J. E. Hilton, and P. W. Cleary, Defining random loose packing for nonspherical grains, Phys. Rev. E **83**, 051305 (2011).

[28] Y. Yuan, Y. Jiao, Y. Wang, and S. Li, Universality of jammed frictional packing, Phys. Rev. Res. **3**, 033084 (2021).

[29] Z. Tian, K. Dong, and A. Yu, Local rotational symmetry in the packing of uniform spheres, Phys. Chem. Chem. Phys. **19**, 14588 (2017).

[30] S. Jiang and M. Li, Local crystalline order features in disordered packings of monodisperse spheres, J. Phys.: Condens. Matter **33**, 205401 (2021).

[31] M. Blétry, Structural diversity of random aggregates of identical spheres, J. Phys. A: Math. Theor. **54**, 045003 (2021).

[32] J. C. Petit, X. García, I. Sánchez, and E. Medina, Contact angle entropy and macroscopic friction in noncohesive two-dimensional granular packings, Phys. Rev. E **96**, 012902 (2017).

[33] W. Wu, G. Ma, W. Zhou, D. Wang, and X. Chang, Force transmission and anisotropic characteristics of sheared granular materials with rolling resistance, Granular Matter **21**, 88 (2019).

[34] S. Papanikolaou, C. S. O'Hern, and M. D. Shattuck, Isostaticity at frictional jamming, Phys. Rev. Lett. **110**, 198002 (2013).

[35] D. P. Haughey and G. S. G. Beveridge, Local voidage variation in a randomly packed bed of equal-sized spheres, Chem. Eng. Sci. **21**, 905 (1966).

[36] J. G. Berryman, Random close packing of hard spheres and disks, Phys. Rev. A **27**, 1053 (1983).

[37] F. Rietz, C. Radin, H. L. Swinney, and M. Schröter, Nucleation in sheared granular matter, Phys. Rev. Lett. **120**, 055701 (2018).

[38] H. A. Vinutha and S. Sastry, Disentangling the role of structure and friction in shear jamming, Nat. Phys. **12**, 578 (2016).

[39] A. V. Anikeenko, N. N. Medvedev, and T. Aste, Structural and entropic insights into the nature of the random-close-packing limit, Phys. Rev. E **77**, 031101 (2008).

[40] M. Saadatfar, H. Takeuchi, V. Robins, N. Francois, and Y. Hiraoka, Pore configuration landscape of granular crystallization, Nat. Commun. **8**, 15082 (2017).

[41] E. R. Nowak, J. B. Knight, E. Ben-Naim, H. M. Jaeger, and S. R. Nagel, Density fluctuations in vibrated granular materials, Phys. Rev. E **57**, 1971 (1998).

[42] F. C. Frank and J. S. Kasper, Complex alloy structures regarded as sphere packings. I. Definitions and basic principles, Acta Crystallogr. **11**, 184 (1958).

[43] T. Speck, A. Malins, and C. P. Royall, First-order phase transition in a model glass former: Coupling of local structure and dynamics, Phys. Rev. Lett. **109**, 195703 (2012).

[44] F. Turci, G. Tarjus, and C. P. Royall, From glass formation to icosahedral ordering by curving three-dimensional space, Phys. Rev. Lett. **118**, 215501 (2017).

[45] S. Zhao and M. Schroter, Measuring the configurational temperature of a binary disc packing, Soft Matter **10**, 4208 (2014).

[46] A. Baule, R. Mari, L. Bo, L. Portal, and H. A. Makse, Mean-field theory of random close packings of axisymmetric particles, Nat. Commun. **4**, 2194 (2013).

[47] J. T. Clemmer, J. M. Monti, and J. B. Lechman, A soft departure from jamming: The compaction of deformable granular matter under high pressures, Soft Matter **20**, 1702 (2024).

[48] J. Li, Y. Cao, C. Xia, B. Kou, X. Xiao, K. Fezzaa, and Y. Wang, Similarity of wet granular packing to gels, Nat. Commun. **5**, 5014 (2014).

[49] K. Shundyak, M. van Hecke, and W. van Saarloos, Force mobilization and generalized isostaticity in jammed packings of frictional grains, Phys. Rev. E **75**, 010301(R) (2007).

[50] F. Xiong, P. Wang, A. H. Clark, T. Bertrand, N. T. Ouellette, M. D. Shattuck, and C. S. O'Hern, Comparison of shear and compression jammed packings of frictional disks, Granular Matter **21**, 109 (2019).